J Neurophysiol 106: 1888–1900, 2011.
First published July 13, 2011; doi:10.1152/jn.00165.2011.

Contrast sensitivity of MT receptive field centers and surrounds

James M. G. Tsui and Christopher C. Pack
Montreal Neurological Institute, McGill University, Montreal, Quebec, Canada

Submitted 25 February 2011; accepted in final form 6 July 2011

Tsui JM, Pack CC. Contrast sensitivity of MT receptive field centers and surrounds. *J Neurophysiol* 106: 1888–1900, 2011. First published July 13, 2011; doi:10.1152/jn.00165.2011.—Neurons throughout the visual system have receptive fields with both excitatory and suppressive components. The latter are responsible for a phenomenon known as surround suppression, in which responses decrease as a stimulus is extended beyond a certain size. Previous work has shown that surround suppression in the primary visual cortex depends strongly on stimulus contrast. Such complex center-surround interactions are thought to relate to a variety of functions, although little is known about how they affect responses in the extrastriate visual cortex. We have therefore examined the interaction of center and surround in the middle temporal (MT) area of the macaque (*Macaca mulatta*) extrastriate cortex by recording neuronal responses to stimuli of different sizes and contrasts. Our findings indicate that surround suppression in MT is highly contrast dependent, with the strongest suppression emerging unexpectedly at intermediate stimulus contrasts. These results can be explained by a simple model that takes into account the nonlinear contrast sensitivity of the neurons that provide input to MT. The model also provides a qualitative link to previous reports of a topographic organization of area MT based on clusters of neurons with differing surround suppression strength. We show that this organization can be detected in the gamma-band local field potentials (LFPs) and that the model parameters can predict the contrast sensitivity of these LFP responses. Overall our results show that surround suppression in area MT is far more common than previously suspected, highlighting the potential functional importance of the accumulation of nonlinearities along the dorsal visual pathway.

contrast response function; middle temporal area; surround suppression

MANY VISUAL NEURONS exhibit surround suppression, which is defined operationally as a decrease in spiking response as stimulus size is increased. Surround suppression has been observed at nearly every stage of visual processing, from the retina (Hartline 1940) to the extrastriate cortex (Allman et al. 1985). Functionally it is likely to serve a number of purposes, including redundancy reduction (Atick 1992), noise rejection (Chen et al. 2006), figure-ground segmentation (Allman et al. 1985), and feature detection (Hubel and Wiesel 1965). It may also be useful as a probe of more generic functions of cortical networks, such as normalization and gain control (Heeger 1992). Despite these important functional roles, the mechanisms underlying surround suppression can be difficult to quantify, as they exert nonlinear influences on neuronal responses.

Typically one characterizes the strength of suppression by presenting a neuron with high-contrast stimuli of various sizes and recording a decrease in response as the stimulus extends beyond the excitatory receptive field center. Quantitative studies have led to models in which the center and the surround differ in size and strength (e.g., DeAngelis et al. 1992) and interact through subtractive or divisive operations, with the two formalizations yielding very similar conclusions (Cavanaugh et al. 2002). An important property of these models is that the center and the surround have differential contrast sensitivity, so that the influence of the surround changes with contrast (Anderson et al. 2001; Angelucci et al. 2002; Cavanaugh et al. 2002; Pack et al. 2005; Sceniak et al. 1999). As a result, a mechanistic understanding of center-surround interactions requires knowledge of the contrast sensitivity of the different receptive field components.

Compared with their thalamic inputs, V1 neurons exhibit contrast response functions that are quite nonlinear, particularly in those neurons that project to the most thoroughly studied extrastriate region, the middle temporal area (MT; Movshon and Newsome 1996). In MT ~50% of the neurons exhibit surround suppression that weakens substantially at very low contrast (Pack et al. 2005). However, no study has fully characterized the strength of surround suppression as a function of stimulus contrast in MT. This manipulation is particularly important, as the nonlinear contrast sensitivity in the inputs to MT makes it difficult to predict how the two receptive field components will shape MT responses to any particular stimulus.

Here we have measured the contrast sensitivity of MT neurons to stimuli of varying sizes. We find that many MT neurons that would be classified as lacking surround suppression at high contrast exhibit significant surround suppression at intermediate contrasts. We show with a simple model that this phenomenon can result from the nonlinear contrast sensitivity of MT inputs. In particular, our model shows how high contrast sensitivity in the surround can actually reduce surround suppression under the stimulus conditions typically used to study MT neurons. We conclude that surround suppression in MT is more common than previously suspected and that the different cell classes observed with high-contrast stimuli are likely to reflect the nonlinear sensitivity of surround mechanisms.

METHODS

Animal preparation. Two male rhesus macaque monkeys underwent a sterile surgical procedure to implant a headpost and recording cylinder. After recovery, monkeys were seated comfortably in a primate chair (Crist Instruments) and trained to fixate a small red spot on a computer monitor in return for a liquid reward. Eye position was monitored at 200 Hz with an infrared camera (SR Research) and required to be within 2° of the fixation point in order for the reward to be dispensed. All aspects of the experiments were approved by the Animal Care Committee of the Montreal Neurological Institute and were in compliance with regulations established by the Canadian Council on Animal Care.

Address for reprint requests and other correspondence: C. C. Pack, Montreal Neurological Inst., McGill Univ., 3801 University St., Montreal, QC H3A 2B4, Canada (e-mail: christopher.pack@mcgill.ca).

We recorded from well-isolated single neurons in area MT. Single waveforms were sorted online and then resorted offline with spike-sorting software (Plexon). Area MT was identified based on anatomic MRI scans, the prevalence of direction-selective neurons, and the correlation between receptive field size and eccentricity. After our initial exploration of MT in each monkey, subsequent recordings were targeted preferentially toward sites where we found neurons with small receptive field eccentricities. This allowed us to explore the surrounds more fully in the context of a visual display monitor of limited size.

Procedure and visual stimuli. Once a neuron was isolated, we first determined its preferred direction of motion manually by presenting a moving bar and delimited the visual area that was responsive to the stimulus. Next, we determined the center of the receptive field by moving a small, drifting grating inside the receptive field and by identifying the area where the stimulus evoked the strongest activity. We then manually fine-tuned the grating parameters to determine the optimal size. The preferred speed was obtained by first manually picking the spatial frequency and then adjusting the temporal frequency to evoke the strongest activity from the neuron. Subsequently, we obtained a direction tuning measurement with the optimal drifting sinusoidal grating stimulus centered on the receptive field. Prior to motion onset, the grating remained stationary for 200 or 250 ms, after which it began moving in 1 of 12 randomly interleaved directions spaced around the circle at 30° intervals for either 400 ($n = 108$) or 500 ($n = 63$) ms. The grating stimuli prior to motion onset and during motion were oriented orthogonally to the direction of motion. For the main experiment we tested each cell with grating stimuli moving at the preferred speed and in the preferred direction, as determined from the direction tuning curve. The stimulus duration for the size tuning experiments was the same as that used for the direction tuning. On each stimulus presentation, the stimulus radius was chosen from a range of possible values (2–17° or 1–15° in steps of 3° or 2°, respectively) and contrasts [1–64% in logarithmic steps (1%, 2%, 4%, 8%, 16%, 32%, and 64%, $n = 31$); for an additional 30 cells we also used gratings of 100% contrast], with all combinations interleaved in blockwise random fashion ($n = 61$). For a larger population of 110 neurons, we measured size tuning functions at two contrasts, chosen to be high (100%) and intermediate (5% or 10%). Each stimulus was repeated five times.

Stimuli were displayed at 75 Hz and a spatial resolution of 1,920 × 1,200 pixels on a Dell 2707WFP LCD monitor, which provided a viewing area of 70° × 42° of visual angle at a distance of 42 cm. Stimuli consisted of grating patches displayed on a gray background (mean luminance of 70.3 cd/m^2) in the center of the receptive field of the neuron under study.

Data analysis. We first characterized the direction selectivity for each neuron by fitting the direction tuning curves at high contrast to a von Mises function. Only the neurons with direction tuning curves that fit statistically better to a von Mises function than to a straight line defined by the average evoked responses were included in the analysis (F-ratio test, $P < 0.05$; 8 cells did not meet this criterion).

For the size tuning curves, the response of each neuron to a given stimulus was quantified as the average spike count in a time window of 200 ms that provided the strongest activity after motion onset. This metric was chosen because it does not require assumptions about response latency, which varied widely across stimulus sizes and contrasts (2-way ANOVA, no significant interaction; main effect of size $F = 10.931$, $P = 0.001$ and contrast $F = 8.12$, $P < 0.001$). We also analyzed the data with a fixed time window near the end of the response and the average response across a time period equal to the duration of the stimulus. The three methods yielded similar conclusions (compare Fig. 1 with Supplemental Fig. S1, *a* and *b*) with respect to surround suppression and its interaction with stimulus contrast.[1]

For some cells the size tuning curves did not have a clear asymptote, indicating that we had not probed the full extent of the center and/or surround. To identify these neurons, we performed bootstrap tests on the data points collected at the three largest sizes. The spike rates were resampled with replacement 2,000 times; each time we performed a linear regression and calculated the slope. A neuron was discarded if the mean of the distribution of slopes differed significantly from zero ($P < 0.05$). In total, 32 cells were discarded from further analysis ($n = 9$ for multiple contrasts, $n = 23$ for 2 contrasts only).

For the remaining cells, the size tuning curves for each contrast condition were then fitted to Gaussian and difference of Gaussians (DOG) models (Sceniak et al. 1999). The former model simulates the property of a cell that lacks a suppressive surround and is given by the following equation:

[1] Supplemental Material for this article is available online at the Journal website.

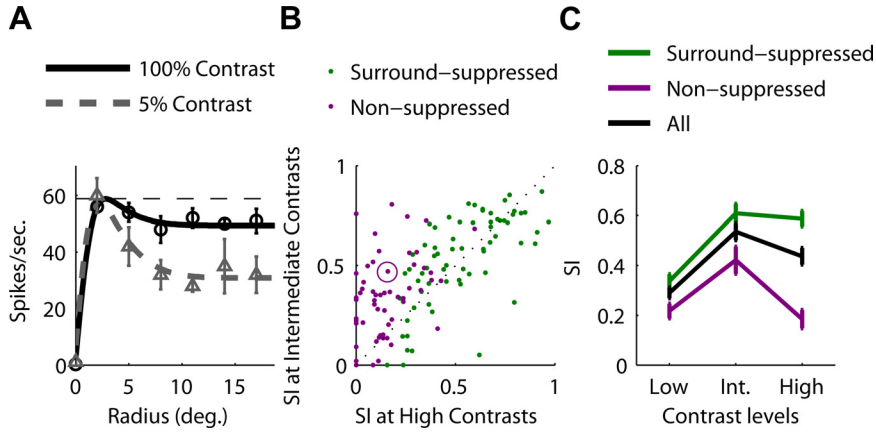

Fig. 1. Effect of stimulus contrast on surround suppression in middle temporal area (MT). *A*: size tuning of an example cell. The responses show a modest decrease with increasing stimulus size for high (100%; ○)-contrast stimuli but a large size-dependent suppression for intermediate (5%; △)-contrast stimuli. Lines show the results of fitting a difference of Gaussians (DOG) model to the data. Horizontal dashed line shows the peak response of the cell. Error bars in this and all subsequent figures show standard error. *B*: effect of contrast on the suppression index (SI) for 133 MT cells. Cells showing weak suppression at high contrast ("nonsuppressed," purple dots; $n = 66$) become significantly more suppressed at intermediate contrast. This trend was not observed for the cells that showed strong suppression at high contrast ("surround suppressed," green dots; $n = 67$). Circled dot corresponds to example neuron in *A*. *C*: SI as a function of contrast. Purple line shows average SI for nonsuppressed cells at low (≤4%), intermediate (8%), and high (≥64%) contrasts. Suppression peaks at intermediate contrast. Average SI for surround-suppressed cells (green line) increases and stabilizes at intermediate contrast. Black line shows average SI for entire population.

$$R_G(s) = A_e erf\left(\frac{s}{a}\right) + R_0 \quad (1)$$

where s, A_e, a, and R_o are the radius of the stimulus, the excitatory amplitude, the size of the excitatory receptive field, and the spontaneous firing rate; *erf* is the error function. The second model describes the subtractive interaction between the excitatory center and the inhibitory surround:

$$R_{DOG}(s) = A_e erf\left(\frac{s}{a}\right) - A_i erf\left(\frac{s}{b}\right) + R_0 \quad (2)$$

with A_i and b corresponding to the amplitude and the size of the inhibitory surround (Raiguel et al. 1995; DeAngelis and Uka 2003). This method allows us to investigate the spatial extent of the center and surround (see Supplemental Fig. S2). Neurons were then classified as surround suppressed if the DOG model improved the fit significantly at high contrast (sequential F-ratio test, $P < 0.05$; DeAngelis and Uka 2003). The extent to which each neuron was surround suppressed was quantified by the suppression index (SI), defined as the ratio of the difference in the responses evoked by the optimal (R_{opt}) and the largest (R_{large}) stimuli to the response evoked by the optimal stimulus:

$$SI = \frac{R_{opt} - R_{large}}{R_{opt}} \quad (3)$$

While this method provides a reasonable measure of suppression, it is undesirably subject to noise at the optimal and at the largest data points. Thus, for the SI calculations, we defined the responses based on the fits to the DOG model, which captures the general trend of the size tuning profile. Similar results were obtained when we performed the analysis on the raw responses (Supplemental Fig. S1*c*).

To estimate the temporal dynamics of the SI, we first computed the time responses for each cell at the optimal size (defined as the size at which the response reaches 95% of its peak) and at the largest size. The time responses were obtained by convolving the spike times with a Gaussian filter ($\sigma = 10$ ms). We then calculated the time course of the SI as follows:

$$SI(t) = \frac{R_{opt}(t) - R_{large}(t)}{R_{opt}(t)} \quad (4)$$

where $R_{opt}(t)$ and $R_{large}(t)$ are the responses at the optimal and largest sizes, respectively.

Model. As in other visual areas (e.g., V1; DeAngelis et al. 1994), MT receptive field centers and surrounds overlap spatially. Thus the contributions of the center and surround cannot be determined directly from the spiking output of a neuron, but rather must be estimated from a model that has parameters corresponding to each receptive field component. We therefore fit our data to a modified version of the DOG model that produces a response to stimuli of different sizes as well as contrasts. The general form of the model is given by:

$$R_{modDOG}(c, s) = R_e(c, s) - R_i(c, s) + R_0 \quad (5)$$

where $R_e(c,s)$ and $R_i(c,s)$ are the excitatory and inhibitory components and R_0 is the spontaneous firing rate. The excitatory component is defined as follows:

$$R_e(c, s) = \frac{k_e(\alpha(s)c)^n}{(\alpha(s)c)^n + {c_{50n}}^n} \quad (6)$$

where k_e, n, and c_{50n} are the gain, the slope, and the semisaturation constant of the excitatory contribution to the contrast-size response. To determine a functional form for the size dependence of neural responses, we performed preliminary investigations in which the size response α was fitted nonparametrically with a different value for every size (see Supplemental Fig. S3). The results indicated that the size response functions of both the center and surround took on a sigmoidal shape. Thus we defined α as follows:

$$\alpha(s) = \frac{k_a}{1 + e^{a_n(a_{50} - s)}} + a_0 \quad (7)$$

where k_a, a_n, a_{50}, and a_0 are the gain, the slope, the response threshold, and the baseline response of the excitatory receptive field. The advantage of this formulation over the more standard error function was that the sigmoid function introduced a threshold (via the parameter a_{50}) below which the surround had little influence (see also Raiguel et al. 1995). A similar approach has been found to be useful in modeling V1 surrounds (Angelucci et al. 2002).

The terms of the excitatory component in *Eq. 6* can be rearranged algebraically to yield

$$R_e(c, s) = \frac{k_e c^n}{c^n + \left(\frac{c_{50n}}{\alpha(s)}\right)^n} \quad (8)$$

which provides a measure of the semisaturation constant

$$C_{50}(s) = \frac{c_{50n}}{\alpha(s)} \quad (9)$$

of this component at different stimulus sizes.

The inhibitory component was defined analogously as follows:

$$R_i(c, s) = \frac{k_i c^m}{c^m + \left(\frac{c_{50m}}{\beta(s)}\right)^m} \quad (10)$$

where

$$\beta(s) = \frac{k_b}{1 + e^{b_n(b_{50} - s)}} + b_0 \quad (11)$$

yielding a total of 15 parameters for each cell. Only the cells with $R^2 > 0.6$ (variance accounted for, equal to the square of the correlation coefficient between the model fit and measured responses) were included in this study (46/52). Our model resembles those described in Tadin and Lappin (2005), with the important difference being the nonseparability of the effects of contrast and size.

RESULTS

We analyzed the responses of 133 MT neurons to stimuli of varying contrast and size in two alert, fixating macaque monkeys. For a subset of these recordings ($n = 46$) we examined many combinations of contrast and size, and these data were fit with a model that provided estimates of the individual center and surround contributions.

Effects of contrast on suppression strength. Figure 1*A* shows the responses of an example neuron, which had a receptive field eccentricity of 5.7°, to stimuli ranging in radius from 0 to 17°. The symbols show the mean neuronal responses, and the lines show the fits of a standard DOG model (Sceniak et al. 1999) to the data. The standard model is based on the assumption that the receptive field is composed of a surround that overlaps the center and inhibits it via subtraction, and the model fits result from optimizing the size and strength of each receptive field component. In Fig. 1*A* these parameters are chosen separately for each contrast.

In light of its responses to high-contrast (100%) stimuli, the neuron appears to have weak surround suppression, as its response is similar for all stimuli larger than ~2° in radius (Fig. 1*A*). However, when the cell was tested with stimuli of

intermediate (5%) contrast, surround suppression emerged (Fig. 1*A*), indicating that the cell actually had an inhibitory surround that would have been missed if we had only studied it with high-contrast stimuli. Thus the responses of this neuron depended on a rather complex interaction between stimulus size and contrast.

Figure 1*B* plots the SI (defined in METHODS), which captures the strength of suppression for large stimuli, for the population of MT neurons tested at high (≥64%) and intermediate (5–10%) contrasts. For comparison with previous literature, we have divided the cells into those that showed statistically significant surround suppression (defined in METHODS) at high contrast ("surround suppressed," $n = 67$) and those that did not ("nonsuppressed," $n = 66$). The nonsuppressed cells generally become more surround suppressed at intermediate contrast, and this trend was statistically significant (paired *t*-test, $P < 0.00001$). Note that this is not a consequence of noise in the measurement of surround suppression, as this would cause a decrease in suppression for the surround-suppressed neurons, which was not observed (*t*-test, $P = 0.905$). In total 44% (29/66) of the cells that appeared to lack surround suppression at high contrast exhibited statistically significant (sequential *F*-test, $P < 0.05$) suppression at intermediate contrast. This was not due simply to the scheme by which cells were classified at high contrasts, as the trend toward stronger suppression at intermediate contrasts was found across the population (Fig. 1*B*; paired *t*-test, $P < 0.00001$).

Figure 1*C* summarizes these results by plotting the average SI for low (≤4%), intermediate (8%), and high (≥64%) contrasts. As in the example cell in Fig. 1*A*, surround suppression for nonsuppressed cells peaks for intermediate contrast and declines for higher contrasts. This effect is not observed for the surround-suppressed cells. In general the increase in surround strength (defined by the change in SI from high to intermediate contrast) was inversely correlated with receptive field eccentricity (Spearman's ρ; $r = -0.277$, $P = 0.0013$), presumably because the surrounds of more foveal cells were more fully stimulated by the limited field of our visual display. This may explain why a recent study that focused on larger receptive field eccentricities did not find significant differences between suppression strength at high and intermediate contrast in MT (Hunter and Born 2011).

Effect of contrast on size tuning. A change in the strength of surround suppression must be driven by changes in the firing rates at the optimal or largest stimulus sizes, but the SI metric does not distinguish between these two types of influences. However, the distinction is important, as it bears on the nature of the mechanisms underlying center-surround interactions in MT. One possibility is that increasing stimulus contrast increases the firing rate by roughly the same amount at all stimulus sizes (Fig. 2*A*), which would lead to a rather trivial explanation for the effects shown in Fig. 1*B*. Specifically, adding a constant to the numerator and denominator of the SI computation (*Eq. 3*) would cause the ratio to tend toward unity, which would lead to lower SIs for higher contrasts.

The other possible explanations involve differential modulation of the firing rate at optimal and large stimulus sizes as contrast is increased. Previous work has provided evidence that increasing the contrast can decrease the responses to large stimuli in MT (Pack et al. 2005), so if a similar result were found for optimal stimulus sizes (Fig. 2*B*), it might explain the

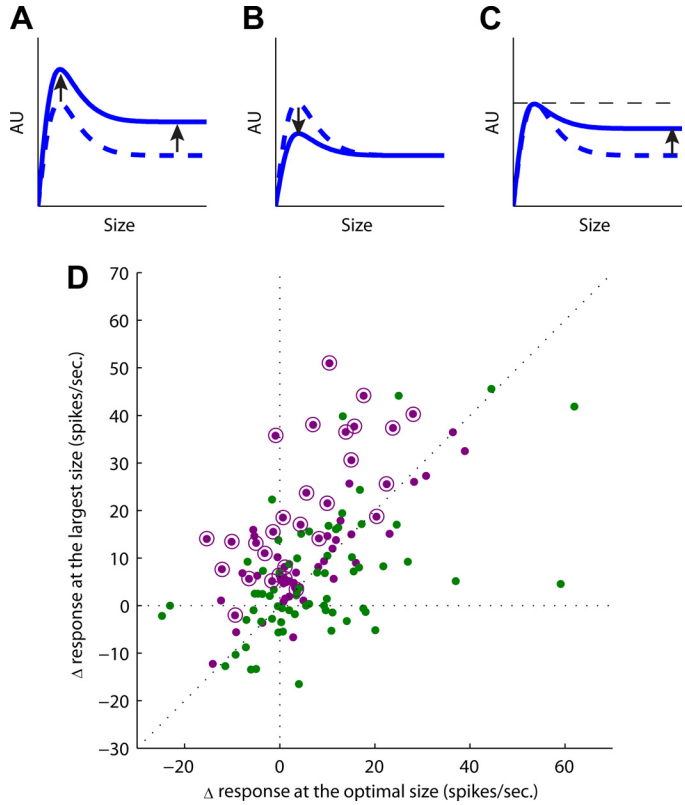

Fig. 2. Effects of contrast on size tuning. *A–C*: simulated size tuning curves from the DOG model illustrating possible scenarios that might lead to a reduction of SI from intermediate (dashed line) to high (solid line) contrasts. AU, arbitrary units. *A*: responses at the optimal and largest sizes increase together with contrast. *B*: response at the optimal size decreases with contrast. *C*: response at the largest size increases with contrast. Horizontal dashed line shows the peak response. *D*: observed changes in response (response at high contrast − response at intermediate contrast) at the largest size plotted against changes in response at the optimal size for the nonsuppressed (purple, $n = 66$) and surround-suppressed (green, $n = 67$) cells. Circled dots show cells that are classified as nonsuppressed at high contrast but surround suppressed at intermediate contrast according to a sequential *F*-test (see METHODS for details).

results described in Fig. 1*B*. The last possibility is that increasing contrast increases the responses to the largest stimuli but not to the optimal stimuli, which would lead to a lower SI (Fig. 2*C*).

The responses of the example cell in Fig. 1*A* are consistent with the last of these hypotheses. Here, the response to a stimulus of optimal size (2° radius) is roughly the same for 5% and 100% contrast. However, the response to the largest size (17°) is highly dependent on contrast, being smaller for the intermediate- than for the high-contrast condition. Thus the stronger surround suppression observed at intermediate contrast appears to be due to a differential effect of contrast at small and large stimulus sizes.

To examine this point in more detail, we used the DOG fit from the neurons shown in Fig. 1*B* and computed the difference in responses of the DOG fit from intermediate to high contrast at the largest size. We then plotted this value on the *y*-axis of Fig. 2*D* against the analogous value for the optimal size. Here, the figure shows that the majority of the points from the nonsuppressed category ($n = 66$) lie above the diagonal line, suggesting that an increase in contrast produces larger changes at the largest size than at the optimal size (paired *t*-test,

$P < 0.001$). This trend is not significant for the surround-suppressed cells (paired t-test, $P = 0.27$, $n = 67$).

The fact that contrast had less effect on the responses to smaller stimuli may indicate that the firing rate was near saturation or had saturated (Fig. 2*C*), and this nonlinearity might provide an explanation for our results. However, for 11 of the cells that became surround suppressed only at intermediate contrast, the activity at the optimal size decreased as contrast increased (see Supplemental Fig. S4, *a* and *b*, for example cells). To investigate this idea further, we also plotted the surround index only for those cells whose peak responses did not occur at the highest contrast ($n = 49$). The results again showed stronger surround suppression at intermediate contrast (Supplemental Fig. S1*d*), ruling out the response saturation explanation.

For some neurons, including the one shown in Fig. 1*B*, the peak response at high contrast occurred for the smallest stimulus size tested. Consequently the estimates of the sizes of their receptive field centers were poorly constrained, and it is possible that high-contrast surround suppression was underestimated for these neurons. However, analysis of the subpopulation of MT neurons for which the peak response occurred at intermediate stimulus sizes yielded the same pattern of contrast-dependent effects seen in the full population (Supplemental Fig. S1*e*; see Supplemental Fig. 4, *c* and *d*, for example cells). This suggests that the results shown in Fig. 1 were not due to undersampling of stimulus sizes.

A model of center-surround interactions. The previous section showed that MT neurons that appear to lack surround suppression for stimuli of very high contrast often exhibit surround suppression for intermediate stimulus contrasts, and that this effect is driven primarily, though not exclusively, by stronger contrast response modulation for the largest stimuli. To understand the mechanisms that might be responsible for these results, we devised a model in which the responses of each neuron were attributable to the interaction of a receptive field center and surround (see METHODS for details). The model involved parameters that corresponded to the size and contrast response of each component (center and surround). The interaction between the center and surround was modeled via subtraction, although we have verified that similar results with respect to all of the main findings reported here are obtained with a divisive model.

Figure 3*A* shows size tuning functions at different stimulus contrasts for an example MT cell. The symbols in each panel correspond to the neuronal responses, and the solid lines correspond to the model fits. The model captures all of the main features of the data ($R^2 = 0.90$), including the nonmonotonic dependence of surround suppression on contrast. Across the population of MT neurons, model fits were similarly quite strong, with a median R^2 value of 0.80 (see Supplemental Fig. S5 for the distribution of R^2 values for the population).

Analysis of the model parameters proved useful for interpreting the counterintuitive effects of contrast on surround suppression. In particular, the model allowed us to estimate the contrast response functions of each neuron's center and surround, which are not readily observable from extracellular recordings. These contrast response functions provide two measures of responsiveness to contrast: the semisaturation constant, which corresponds to the contrast at which the response reaches 50% of its maximum, and the slope of the function, which expresses the speed with which the response changes with increasing contrast. Figure 4*A* shows these contrast response functions for the center and surround of the example neuron shown in Fig. 3*A*. For the smallest stimulus (1° radius), the center has a fairly linear contrast response. Its semisaturation constant decreases slightly when the stimulus size is increased to the size of the receptive field (~3° radius;

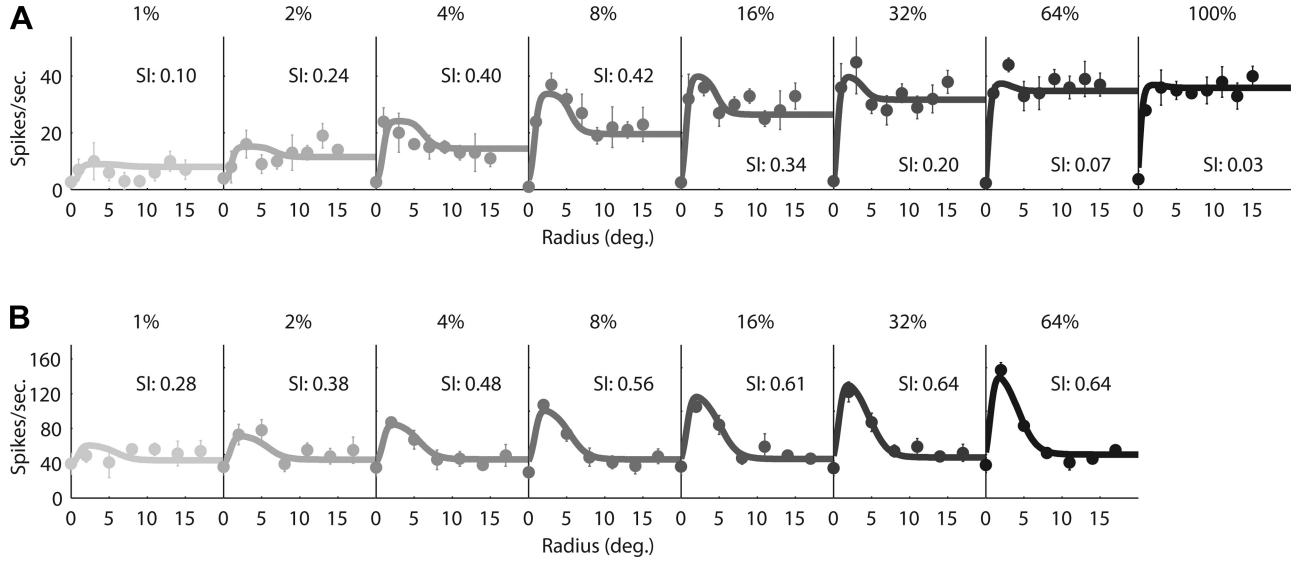

Fig. 3. Example MT cells. *A* and *B*: size tuning curves for different levels of contrast (increasing from *left* to *right* and from light to dark gray). Filled circles show mean neuronal responses, while solid line shows data fitted with the model described in *Eq. 5*. *A*: nonsuppressed example cell. The response at the optimal size rises quickly until 8% contrast, while the response at the largest size increases gradually with contrast. Surround suppression is strongest at intermediate contrast. Model parameters: $k_a = 0.43$, $k_b = 0.50$, $a_{50} = 1.02$, $b_{50} = 6.13$, $a_n = 3.15$, $b_n = 1.08$, $a_o = 0.00$, $b_o = 0.06$, $n = 1.14$, $m = 2.26$, $c_{50n} = 2.31$, $c_{50m} = 2.00$, $k_e = 53.33$, $k_i = 17.77$, and $R_o = 2.14$. Variance accounted for, $R^2 = 0.9$. *B*: surround-suppressed example cell. The response at the optimal size increases gradually with contrast, while the response at the largest size does not change. Model parameters: $k_a = 0.25$, $k_b = 0.30$, $a_{50} = 1.13$, $b_{50} = 6.32$, $a_n = 3.23$, $b_n = 0.93$, $a_o = 0.00$, $b_o = 0.00$, $n = 0.66$, $m = 0.79$, $c_{50n} = 3.92$, $c_{50m} = 3.35$, $k_e = 183.75$, $k_i = 147.33$, and $R_o = 36.04$. Variance accounted for, $R^2 = 0.9$.

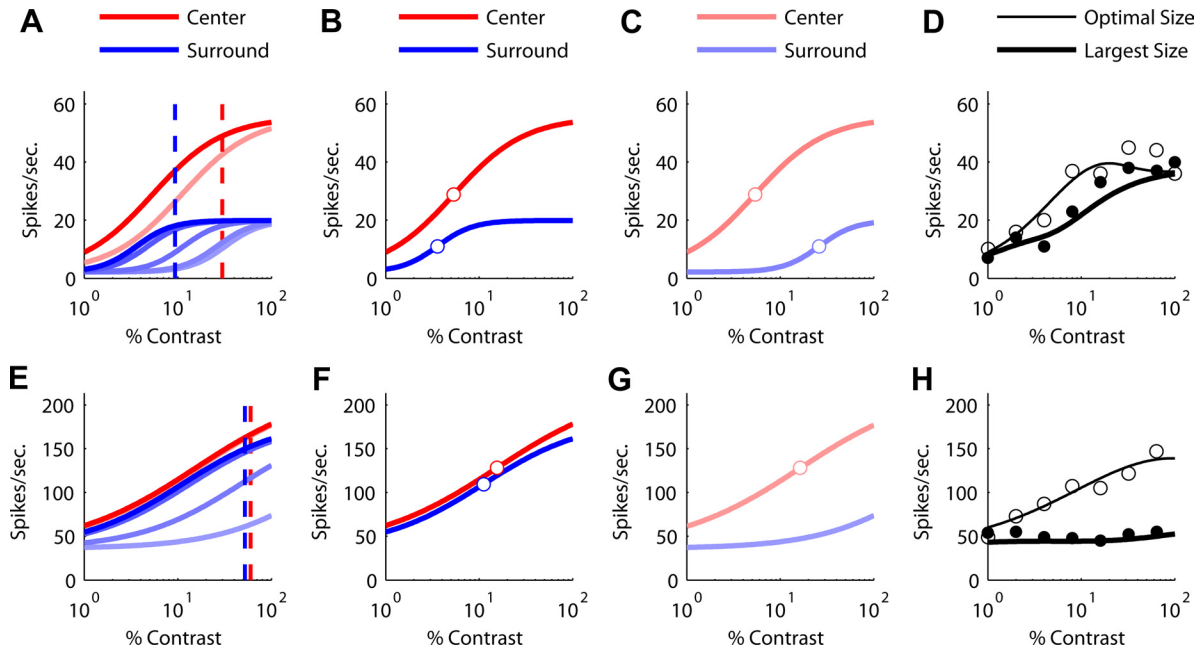

Fig. 4. Center and surround contrast response functions (CRFs) from the fitted model (see *Eq. 5*). *A*: center (red) and surround (blue) contrast responses to different sizes (light: small; dark: large) for the example cell in Fig. 3*A*. As size increases, the CRF of the center unit shifts leftward, indicating increased contrast sensitivity. This shift is more pronounced for the surround component. Red and blue dashed lines show the contrasts at which the center and the surround reach 90% of their maximum responses at the largest size. The surround saturates at a lower contrast than the center. *B*: same as *A*, but for the largest size only. Open circles show the semisaturation constants. *C*: same as *B*, but for the optimal size only. *D*: difference between the center and surround contrast responses and the measured neuronal responses in *A* at the optimal (thin line and open circles) and largest (thick line and filled circles) sizes. *E*: same as *A*, but for the example cell in Fig. 3*B*. Here the center and the surround contrast responses both saturate at high contrast. *F*: same as *B*, but for the contrast responses in *E*. *G*: same as *C*, but for the contrast responses in *E*. *H*: same as *D*, but for the contrast responses in *E*.

Fig. 4*A*), as shown by the leftward shift of the contrast response function (*Eq. 9*; see also Sclar et al. 1990). Extending the stimulus beyond the excitatory receptive field has no effect on this component of the response (by definition).

This neuron's surround exhibits a more dramatic decrease in its semisaturation constant with increasing stimulus size, as shown by the shapes of the blue contrast response functions in Fig. 4*A*. Here darker blue lines correspond to larger stimulus sizes. Its semisaturation constant continues to decrease with increasing stimulus size across a large range of sizes, as shown by the leftward shift of the blue curves in the figure. This suggests that the surround has a much larger spatial extent than the center. For clarity, the contrast response functions for the largest size and optimal size are replotted in Fig. 4, *B* and *C*, respectively. Figure 4*D* plots the difference between the model center and surround contrast response functions and the measured responses at the optimal and largest stimulus sizes.

For the largest stimulus size (Fig. 4*B*), the contrast at which the response begins to increase for the surround is reasonably similar to that of the center, with the two components having C_{50} values (defined in METHODS, *Eq. 9*) of 5.3 and 3.6. However, the center and the surround differ more strongly in the slopes of their contrast response functions: While the center contrast response function rises gradually ($n = 1.14$), that of the surround increases rapidly ($m = 2.26$) and saturates at a lower contrast, as shown in Fig. 4*A*. As the center response continues to increase with contrast beyond this point, the cell exhibits stronger responses at high contrast (Fig. 4*D*).

Conversely, for the optimal stimulus size (Fig. 4*C*), the surround only exerts its suppressive influences at higher contrasts ($C_{50} = 26.2$), while the contrast response of the center changes little compared with that at the largest size ($C_{50} = 5.4$). As contrast increases, the neuron is therefore modulated only by excitatory input up to ~10% contrast, at which point the surround begins to respond. In summary, at optimal stimulus size, the neuronal response first increases rapidly with contrast but levels off at intermediate contrast, while for the largest stimulus, it continues to increase across the range of contrasts.

Figure 4*E* shows the contrast responses of the center and the surround for another example neuron (raw data shown in Fig. 3*B*, $R^2 = 0.90$) that was classified according to standard criteria as surround suppressed. For large stimuli the center and surround responses are nearly parallel across the entire range of contrasts (Fig. 4*F*), suggesting that the overall response at the largest size was mostly independent of contrast. This is shown clearly in Fig. 4*H*, which plots the difference of the center and surround contrast response functions from the model fit and the actual responses to this neuron. At the optimal size, the inhibitory input is negligible (Fig. 4*G*). Consistent with these observations, the cell did not show a decrease in the strength of surround suppression from intermediate to high contrasts (SIs of 0.56 and 0.64, respectively). These results were independent of whether or not the spontaneous firing rate was subtracted from the responses prior to calculation of the SI (Supplemental Fig. S1*f*).

Interaction of center and surround in MT. The preceding analysis suggests that the stronger surround suppression observed at intermediate contrasts results from the leftward shift of the surround contrast response function as size increases, and this is driven by two factors. The first factor is that larger stimuli are associated with a decrease in the semisaturation

constant, as would be expected from previous studies (Sclar et al. 1990). However, this change is greater for the surrounds than for the centers, and this is due simply to the fact that the surrounds are larger and hence more capable of integrating weak signals over space. This result is summarized in Fig. 5*A* for the MT population for which at least seven different contrasts were tested ($n = 46$). Here the average values of C_{50} for the center and the surround are plotted as a function of stimulus size (*Eq. 9*). Note that under conditions in which the contribution of the surround was very small, the value of C_{50} becomes uninterpretable; the means in Fig. 5*A* therefore exclude values of C_{50} that exceeded 100.

The second factor is the significantly higher contrast response slope of the surround (m) compared with that of the center (n; paired t-test, $P < 0.001$, $n = 18$ for nonsuppressed and $P = 0.0039$, $n = 28$ for surround-suppressed cells). For many cells the contrast response of the surround is highly nonlinear, exhibiting saturation at intermediate contrasts (Fig. 4*A*). Thus, beyond a certain contrast, the contribution of the surround is quite limited relative to that of the center, which continues to exhibit increasing responses with increasing contrasts.

Thus one explanation for the counterintuitive interaction of contrast and size is simply that, for many cells, the surround response to a large stimulus saturates at a lower contrast than that of the center. This difference is shown for the example cell by the dashed vertical lines in Fig. 4*A*. To determine whether this explanation holds for the population of neurons shown in Fig. 5*A*, we plotted the relative strength of surround suppression for high and intermediate contrasts against the relative saturation points (defined as the contrast for which the response at a given stimulus size reached 90% of its maximum) for the center and surround (Fig. 5*B*). There is a highly significant correlation [Spearman's ρ; $r = 0.498$, $P = 0.007$ and $r = 0.765$, $P = 0.0003$ for surround suppressed ($n = 28$) and nonsuppressed ($n = 18$), respectively] between these two measures, suggesting that this factor accounts for the observation that intermediate contrasts yield the highest surround suppression.

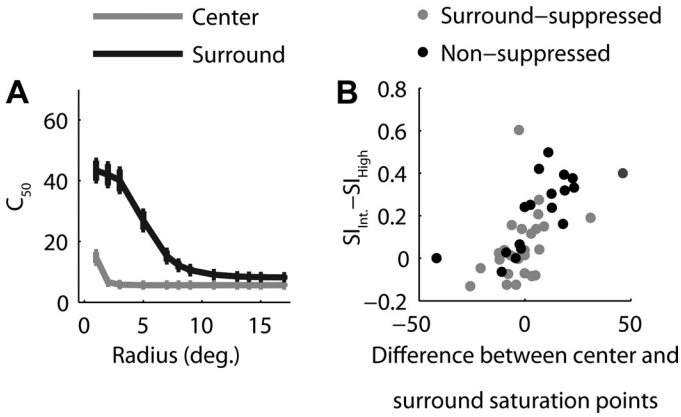

Fig. 5. Contrast sensitivity of MT receptive field centers and surrounds. *A*: average semisaturation constant (C_{50}) as a function of size for the centers (gray) and surrounds (black), as determined from the model fits. The average values of C_{50} ($n = 46$) for the surround are initially high for small sizes and gradually decrease as size increases. The surround sensitivity to contrast increases as the stimulus covers more area. For the center, the average values of C_{50} decrease for small stimuli and plateau thereafter. Values of C_{50} above 100 were excluded from the average. *B*: relationship between the saturation of the contrast response functions at the largest size and the SI. The decrease in SI as contrast increases [intermediate (Int) to high] is plotted against the difference between the center and surround saturation points at the largest size. The positive correlation suggests that the contrast effect on SI is driven by the surround saturating at lower contrast (surround suppressed $n = 28$, nonsuppressed $n = 18$).

Cell classification. Our results suggest that the apparent lack of surround suppression in many MT neurons results paradoxically from the fact that these neurons have surrounds that are in a sense more sensitive to contrast than the rest of the MT population. Specifically, cells that appear to lack surround suppression often have surround contrast response functions with very high slopes (m), leading to saturation at intermediate stimulus contrasts. The discovery of inhibitory surrounds in these neurons is somewhat surprising in light of previous findings showing that the classification of individual MT neurons as suppressed or nonsuppressed (based on testing with high-contrast stimuli) yields clear topographic clustering (Born and Tootell 1992), distinct anatomic projections (Berezovskii and Born 2000), differential effects on behavior (Born et al. 2000), and consistency with human psychophysical results (Churan et al. 2009). To reconcile these previous results with the present findings we examined the distributions of model parameters with respect to the previously defined categories of cells.

We first divided the cells (same subset as Fig. 5*A*, $n = 46$) into suppressed and nonsuppressed categories, on the basis of their responses to high-contrast stimuli, using standard statistical criteria (Churan et al. 2008; DeAngelis and Uka 2003). This yielded two distributions of model parameters that allowed us to examine the sizes and responsiveness of the receptive field components in the two cell classes. Of the parameters in the model, six yielded a significant difference between surround-suppressed ($n = 28$) and nonsuppressed ($n = 18$) classes (Fig. 6, see also Supplemental Table S1).

For the receptive field centers, we found that surround-suppressed cells had lower response thresholds (a_{50}, $P = 0.02$) and higher slope (a_n, $P < 0.0001$; Fig. 7*A*). In addition, the inhibitory surround baseline of the surround-suppressed cells was also found to be lower (b_o, $P = 0.003$). Thus for very small stimuli the surround has negligible influence (Fig. 7*B*). Taken together, the results suggest that the surround-suppressed cells are more responsive to small stimuli, which is consistent with the finding (Churan et al. 2008) that surround-suppressed neurons respond more strongly to small stimuli that are presented very briefly.

A more impressive difference between the two cell classes can be seen in the average center and surround contrast response functions recovered by the model. Figure 7, *C* and *D*, show the contrast response functions for large (17°) stimuli for the nonsuppressed and surround-suppressed classes. As mentioned above, the contrast response function of the surround is on average more nonlinear for the nonsuppressed cells (slope parameter m, $P < 0.0001$; Fig. 6), while the strength of the surround is greater for the surround-suppressed cells (k_i, $P < 0.0001$; Fig. 6). The center gain parameter was also found to be stronger (k_e, $P = 0.026$; Fig. 6) for the surround-suppressed cells.

Temporal dynamics. A recent study (Churan et al. 2008) found that surround-suppressed neurons were more effective at discriminating motion direction for briefly presented stimuli. This suggests some potentially interesting temporal dynamics

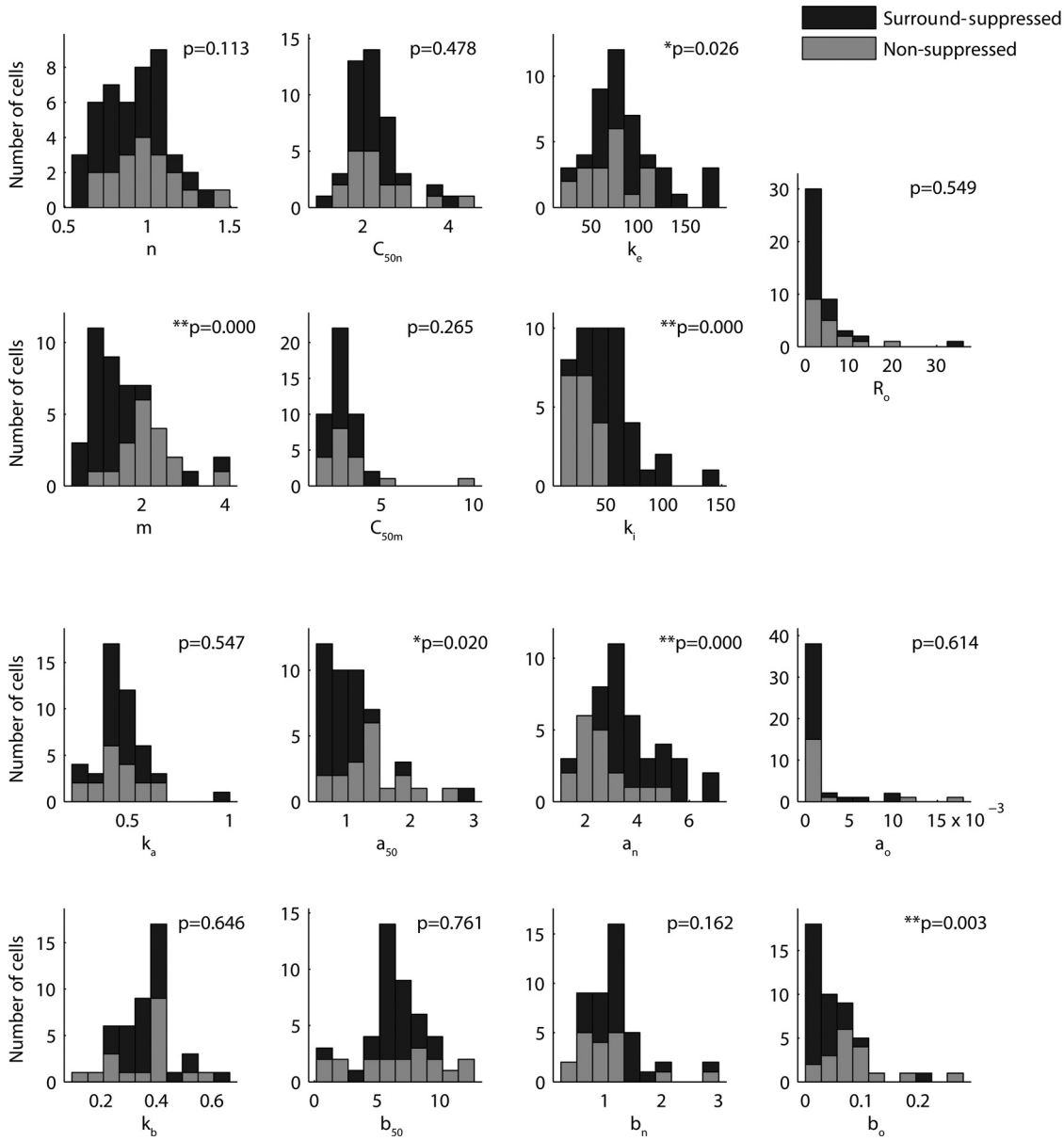

Fig. 6. Distributions of parameters from the model in *Eq. 5* for the surround-suppressed (black) and nonsuppressed (gray) cells of Fig. 5. The parameters that yielded significant differences were the center excitatory strength (k_e), response threshold (a_{50}), slope (a_n), surround inhibitory strength (k_i), contrast slope (m), and baseline response (b_o).

related to surround suppression in MT. We therefore analyzed the temporal responses of 82 neurons for which the stimulus duration was 400 ms (nonsuppressed $n = 36$, surround suppressed $n = 46$). Figure 8, *left*, shows the average temporal responses at the optimal size (defined as the size at which the response reaches 95% of its peak) and at the largest size. For the high-contrast stimuli (Fig. 8, *bottom*), the onset of motion was followed by a strong transient response, as has been reported previously (Priebe et al. 2002). Interestingly, this transient was much higher in amplitude for stimuli of optimal size (Fig. 8), as the responses in other conditions were generally nearly constant across time. Consequently, surround suppression was strongest during the transient period in many cells, leading to a surround index that actually decreased over time. A statistical comparison of surround indices during an early (50–200 ms after motion onset) and a late (200–450 ms) period indicated that the differences were significant (*t*-test, $P < 0.001$ for both classes). This suggests that adaptation mechanisms that are intrinsic to MT (Priebe et al. 2002) reduce the effective strength of surround suppression.

Clustering. An interesting consequence of our model analysis is the prediction that the total excitatory and inhibitory input to the suppressed cells should be greater than the total input to the nonsuppressed cells. This follows from the fact that the excitatory and inhibitory inputs are stronger for the suppressed cells (Fig. 7, *C* and *D*). Moreover, because the suppressed and nonsuppressed cells form separate clusters within MT (Born and Tootell 1992; Born 2000), we would expect this variation in total input to be consistent within area MT over a spatial scale of a few hundred micrometers (Born 2000). This idea can be tested by measuring local field potentials (LFPs), which have been shown to be heavily modulated by the

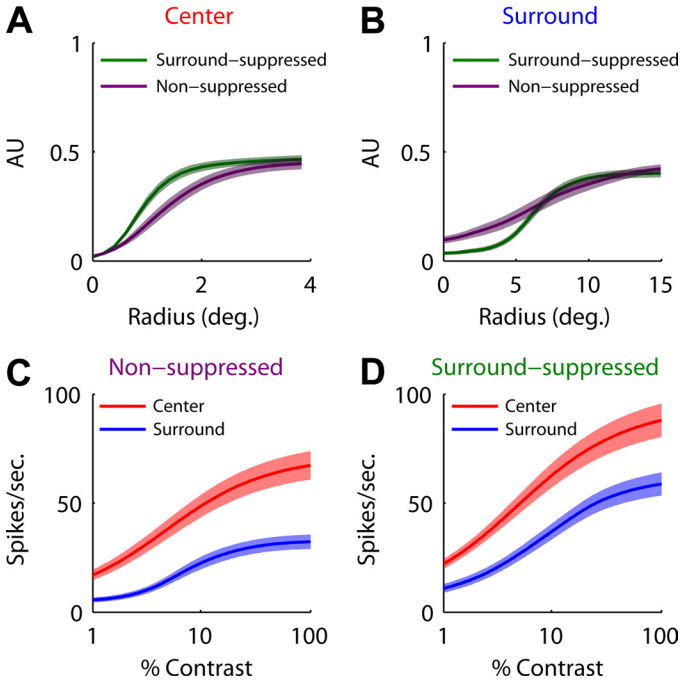

Fig. 7. Average center and surround spatial receptive field structures and contrast response functions from the fitted model (*Eq. 5*); same data set as Fig. 5. *A*: green and purple traces show the average size tuning responses of the receptive field centers for the surround-suppressed ($n = 28$) and nonsuppressed ($n = 18$) cells, respectively. The centers of the surround-suppressed cells are on average more responsive than those of the nonsuppressed cells (see also Fig. 6). *B*: same as *A*, but for the surround. The baseline activity of the nonsuppressed cells is higher than that of the surround-suppressed cells. *C*: red and blue traces show the average center and surround contrast responses, respectively, for cells that lacked suppression at high contrast. *D*: same as *C*, but for cells with strong surround suppression at high contrast.

stimulation of the inhibitory surround of neurons (Gieselmann and Thiele 2008). We therefore analyzed LFP signals that were recorded simultaneously with the single-unit recordings described thus far.

For each suppressed and nonsuppressed single-unit recording we divided the corresponding LFPs into beta (16–24 Hz), low-gamma (25–55 Hz), and high-gamma (65–140 Hz) bands (Khawaja et al. 2009). We then examined these LFP bands along with the spiking outputs for small (1–5°) and large (13–17°) stimuli. Figure 9 shows the results, averaged across the MT population (same subset as Fig. 5; $n = 46$: suppressed sites $n = 28$, nonsuppressed sites $n = 18$). The first row in Fig. 9 shows the mean contrast response function for the spikes: for small stimuli (*left*), responses are generally higher for the suppressed population across the full range of contrasts. The situation reverses for the larger stimuli (*right*), such that the responses of the nonsuppressed group are slightly larger for most contrasts. The second row of Fig. 9 shows the mean difference between the excitatory and inhibitory components of our model for the same cells. This represents the output of the model, and, not surprisingly, the model output provides a good match to the spiking responses on which its parameters were optimized.

The third row of Fig. 9 shows the amplitude of the high-gamma LFP recorded simultaneously with the single-unit activity. In contrast to the spiking outputs, the LFP signals recorded at the surround-suppressed sites are always larger than those recorded at the nonsuppressed sites, even for large stimuli (*right*). Similar results were obtained for the low-gamma LFPs, while the beta-band LFPs show inhibitory effects that are approximately equal for both suppressed and nonsuppressed recording sites (Supplemental Fig. S6). The last row of Fig. 9 shows the sum (rather than the difference as in the 2nd row) of the contrast response functions for the excitatory and inhibitory receptive field components of our model. This manipulation reproduces the main qualitative features of the LFP data: Response amplitude is larger for the suppressed sites across the full range of contrasts and stimulus sizes. Thus our modeling work shows that the single-cell responses in MT can be explained as the difference between an excitatory center and an inhibitory surround, while the LFPs recorded from the same sites are more similar to the sum of these two components.

DISCUSSION

We have examined the interaction of stimulus size and contrast in shaping the responses of MT neurons in macaque visual cortex. Consistent with previous studies (Raiguel et al. 1995; Tanaka et al. 1986), our results indicate that surround suppression is present to some degree in most MT neurons. However, we found that for many neurons that are typically classified as nonsuppressed, surround suppression actually emerges when testing with intermediate contrast stimuli. These results can be accommodated by a simple model that takes into account the nonlinear responses to contrast found in the neurons that provide input to MT. Analysis of the model suggests that cells that appear to lack surround suppression at high contrast do indeed have weaker surrounds, but they also have surrounds that are more nonlinear in their responses to contrast. This latter property leads to the increased suppression seen at intermediate contrasts. Further analysis of the model, using the same parameters obtained from the fits to the single-unit data, provides a qualitative account of the LFP responses, which are consistent with the idea that differences in the strength of inhibitory inputs define the topographic clustering of cells in MT.

Implications for cortical circuitry. Surround suppression examined with extracellular recordings reveals the relative contributions of excitatory and inhibitory mechanisms to the firing rate of the neuron under study. As these mechanisms are likely to differ in overall sensitivity, it is important to characterize them with stimuli of different contrasts. Indeed, previous experiments in V1 have found that contrast shapes the interactions between center and surround in a rather complex fashion (Angelucci et al. 2002; Cavanaugh et al. 2002; Kapadia et al. 1999; Levitt and Lund 1997; Polat et al. 1998), such that the cells cannot be characterized by a single contrast response function or size tuning curve.

Despite this inseparability, many features of the V1 data can be captured by descriptive models with fairly simple components (Cavanaugh et al. 2002), and this is also the case with our MT data. In particular, our model consists only of a receptive field center and surround that are roughly Gaussian in shape and overlapping in space. Both receptive field components simply sum inputs over space, leading to increased contrast sensitivity with increasing stimulus size. This effect is more pronounced in the surround, as it has access to a larger spatial region over which to integrate the stimulus.

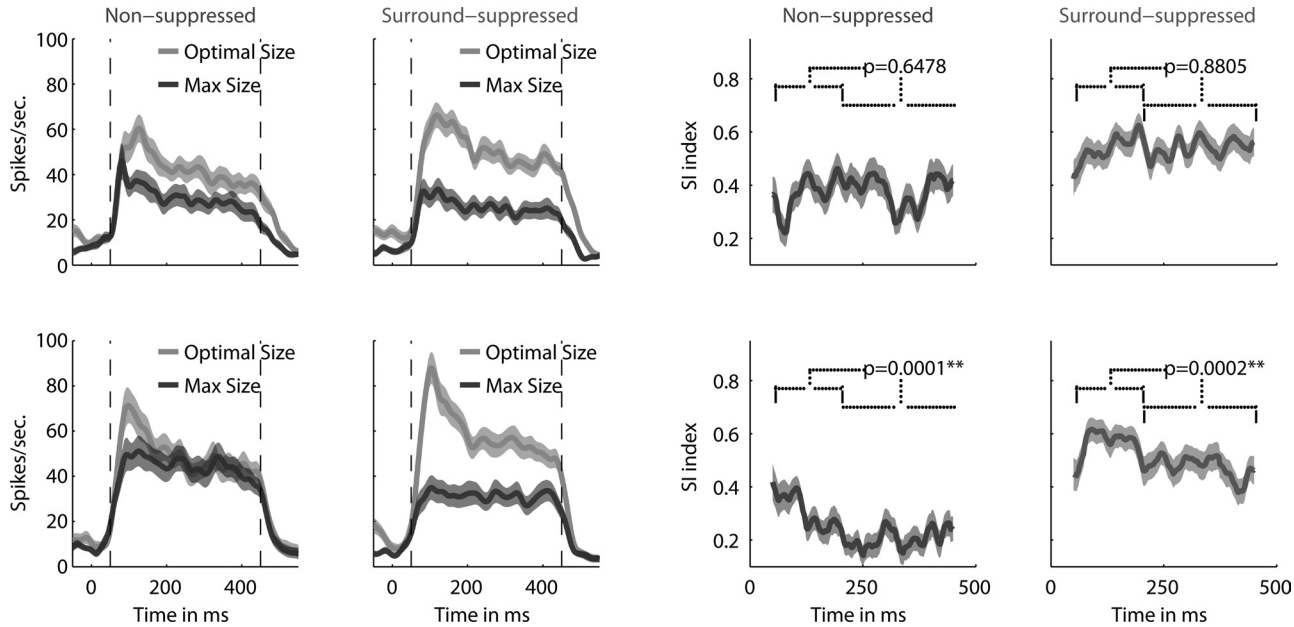

Fig. 8. Temporal dynamics of surround suppression. *Left*: average temporal responses at the optimal size (gray) and at the largest size (black) for the nonsuppressed (*left*, $n = 36$) and surround-suppressed (*right*, $n = 46$) cells for which the stimulus duration was 400 ms. *Right*: time-averaged SI for the nonsuppressed (*left*) and surround-suppressed (*right*) cells. *Top*: results at intermediate contrasts. *Bottom*: at high contrast, there is a significant difference between the average SI measured at different time epochs [50–200 ms (early) and 200–450 ms (late) after motion onset].

One obvious weakness of our model is the assumption of a uniformly distributed radial surround, which is only true for ~25% of the neurons in MT (Xiao et al. 1997). Although such asymmetries may be functionally important (Buracas and Albright 1996), it is unlikely that a more complete mapping of the spatial surround would have changed our conclusions significantly. Previous work has shown that that the fitting errors of the DOG model for neurons with asymmetric surrounds are not significantly different from the fitting errors for neurons with uniform radial surrounds, suggesting that the DOG model provides a reasonable estimate of the radial distribution of the inhibitory field (Raiguel et al. 1995). Another weakness of our model is that we did not take into account the potential effects of differential direction selectivity in the two receptive field components. This may be reasonable, as previous work has suggested that the surround is poorly tuned (Hunter and Born 2011).

Despite the simplicity of the model formulation, its anatomic correlates may involve rather complex connectivity (Schwabe et al. 2006). For grating stimuli of the type used in the present study, the inputs from lower cortical areas are likely to be strongly surround suppressed (Sceniak et al. 2001; Shushruth et al. 2009), so that there is no obvious way to assign a source to the suppression found in the majority of MT cells. However, previous work has shown that the circuits that create surround suppression are similar across lower-level cortical areas (Shushruth et al. 2009), and so by analogy we would expect the suppression found in MT to arise from a combination of feedforward and local sources (Ichida et al. 2007). In this work we have not investigated the possibility of a "far" surround driven by feedback and capable of influencing responses over even larger spatial regions, although such a mechanism would also be expected based on findings in V1 (Ichida et al. 2007). However, our preliminary data showing facilitatory interactions between distant stimuli in the receptive field surround and low-contrast stimuli in the center suggest that the "far" surround may exist in MT as well (Tsui et al. 2009).

Our model of center-surround interactions is based on a standard DOG formulation (DeAngelis and Uka 2003), in which the center and surround overlap spatially. However, for our MT population the contribution of the surround is negligible for very small stimuli centered on the receptive field (Fig. 7*B*). We have interpreted this result based on the notion that the surround has a higher threshold than the center, as in previous work in V1 (Angelucci et al. 2002). However, an alternative explanation would involve a concentric surround that is not activated until the stimulus extends beyond the receptive field center (Raiguel et al. 1995). These two possibilities cannot be distinguished on the basis of the present data set. We note, however, that the DOG model with overlapping center and surround provides a more parsimonious account of the complex motion contrast cells reported by Born (2000). In these neurons, surround suppression is observed for stimuli smaller than receptive field center, as would be expected based on our model.

Previous studies have found evidence for the notion that surround-suppressed and nonsuppressed MT cells exhibit different anatomic clustering and connectivity (Berezovskii and Born 2000; Born and Tootell 1992) in New World monkeys. In Old World monkeys the anatomic arrangement is likely to be more complex, but the results of a microstimulation study in the macaque (Born et al. 2000) indicate that clustering based on surround strength is likely to be present in that species as well (for a full discussion of these issues, as well as potential species differences, see Born and Bradley 2005). Our LFP results (Fig. 9) are consistent with this idea. In particular, the classification of single-unit recording sites as suppressed or nonsuppressed at high contrast predicts the sensitivity of the gamma-band LFPs to stimulus contrast, and this result is consistent with the idea that power in the LFP gamma band

reflects both excitatory and inhibitory synaptic currents (Gieselmann and Thiele 2008). Indeed, we have found that the gain of center and surround responses tend to covary (Fig. 7), which is likely to reflect a general mechanism for shaping stimulus selectivity (Murphy and Miller 2009). An alternative possibility that is also consistent with our results is that the LFPs overrepresent inhibitory currents (Henrie and Shapley 2005). Although the exact spatial area over which LFPs integrate these inputs is a matter of debate, our results suggest that this integration radius is small enough to preserve functional differences between suppressed and nonsuppressed neuronal clusters, which are on the order of a few hundred micrometers (Born 2000).

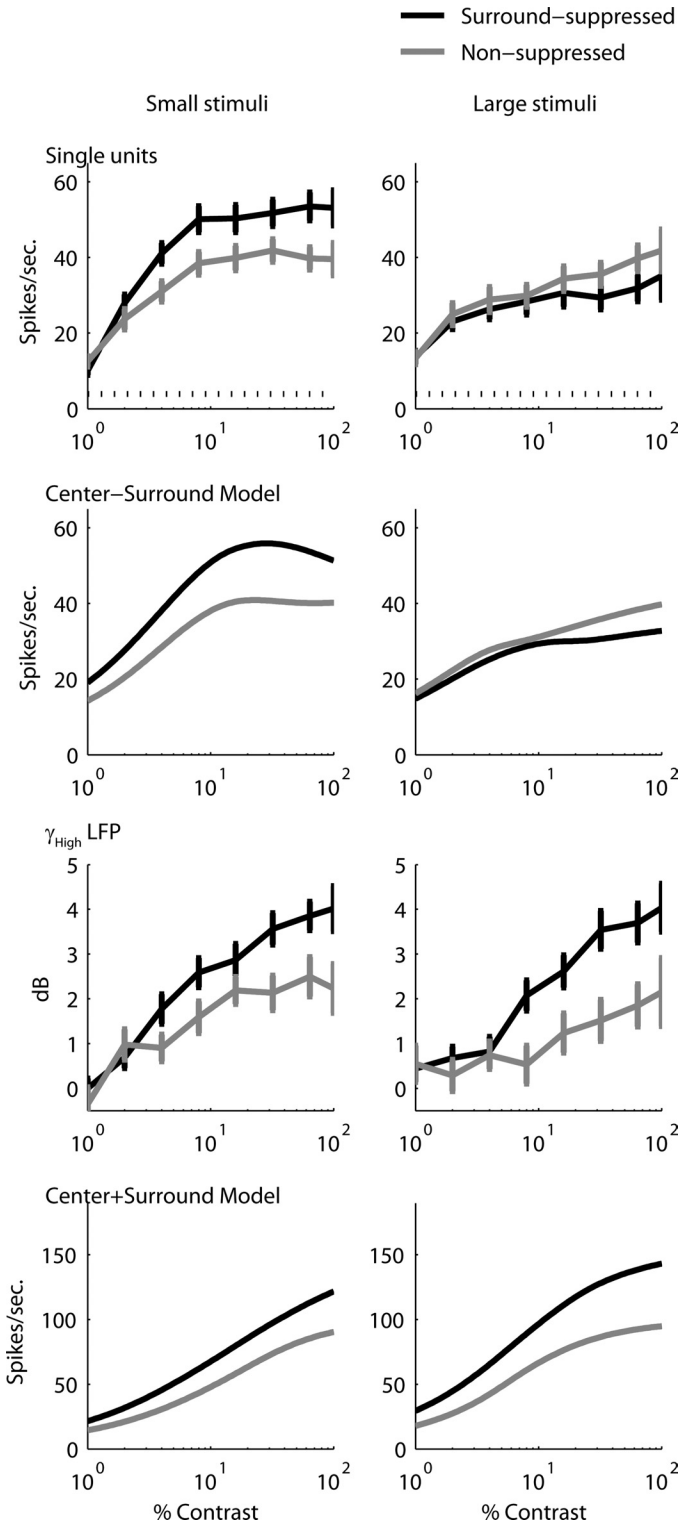

Fig. 9. Mean CRFs for surround-suppressed (black) and nonsuppressed (gray) populations in response to small (≤5°, *left*) and large (≥13°, *right*) stimuli. The first row shows the results for the spikes. At small sizes, the response of the surround-suppressed cells is higher than that of the nonsuppressed cells across a broad range of contrasts. This pattern reverses for large sizes (*right*). Dotted lines show the spontaneous firing rate. The difference in output between the model center and surround captures this trend (2nd row). The third row shows the CRFs for the local field potential (γ_{high} LFP: 65–140 Hz) recorded from sites that had single units with suppressed (black) and nonsuppressed (gray) responses at high contrast. LFP responses for the surround-suppressed population are larger than those for the nonsuppressed population for most contrasts. The bottom row shows the result of adding the center and surround outputs from the model under the corresponding conditions.

Functional implications. Born et al. (2000) showed that microstimulation of suppressed and nonsuppressed clusters of MT neurons in the macaque yielded opposite effects on pursuit eye movements. These results were consistent with earlier speculation based on anatomic clustering in owl monkeys (Born and Tootell 1992) that surround-suppressed neurons are involved in figure-ground discrimination while nonsuppressed neurons are involved in optic flow processing. Our results are generally consistent with this view, provided that the functional roles are defined with respect to high-contrast stimulation. At intermediate contrasts the distinction between the two cell classes becomes rather ambiguous (Fig. 1*B*), and at very low contrasts surround suppression is weakened considerably (Pack et al. 2005). Whether the increased suppression found at intermediate contrasts has any functional utility remains to be seen. Theoretical work has shown that MT surrounds could in principle be useful for inferring shape from motion (Gautama and Van Hulle 2001), estimating surface geometry (Buracas and Albright 1996), and calculating the observer's heading direction (Royden 2002). It would be interesting to determine how these functions are affected by contrast manipulations of the kind we have shown to modulate the strength of MT surrounds.

Regardless of any potential functional utility, the effects of contrast on surround suppression can emerge from a simple model that takes into account the nonlinear contrast sensitivity of V1 neurons. This nonlinearity in turn is thought to reflect mechanisms of normalization and gain control (Heeger 1992) that are present as early as the magnocellular neurons found in the retina and LGN (Kaplan and Shapley 1986). The fact that the nonmonotonic dependence of surround suppression on contrast does not appear in these earlier stages suggests that it results from sequential nonlinear transformations across the visual hierarchy. Importantly, each of these transformations might be quite simple to implement, but the cumulative result in the extrastriate cortex can appear quite complex. Indeed, recent modeling work has shown that much of the stimulus selectivity found in the extrastriate cortex can be viewed as relatively simple transformations of appropriately nonlinear approximations of the output of V1 (Cadieu et al. 2007; Rust et al. 2006; Tsui et al. 2010).

Psychophysical studies have often found that increasing the size, duration, or contrast of a stimulus increases its detectabil-

ity and discriminability (Anderson and Burr 1987, 1989; Henrie and Shapley 2001), but a number of interesting exceptions have been observed. In particular, motion discrimination decreases beyond a certain point with increases in size or contrast (Churan et al. 2009; Tadin et al. 2003; Tadin and Lappin 2005), and such perceptual effects may be attributable to inhibitory surrounds in areas like the human homolog of monkey area MT (Churan et al. 2008). This potential link between mechanisms of surround suppression and perception has motivated further psychophysical studies on subject populations who are thought to have reduced inhibition (Betts et al. 2009; Golomb et al. 2009; Tadin et al. 2006). Typically these studies have focused on comparing perceptual responses to high- and low-contrast stimuli, but a recent study (Betts et al. 2009) has found that in older subjects perceptual surround suppression for motion stimuli is strongest at intermediate contrasts. Thus to the extent that such psychophysical studies provide a measure of inhibitory mechanisms in the brain, it appears that the decline in inhibition seen in some subjects preferentially affects those cells with the strongest inhibitory inputs, causing the perceptual readout to depend more heavily on cells that lack strong suppressive surrounds. In light of these results and the present findings, it would be interesting to reexamine psychophysical correlates of inhibitory influences over a wider range of stimulus contrasts.

ACKNOWLEDGMENTS

We thank Julie Coursol and Cathy Hunt for technical assistance and Rick Born and Nick Hunter for insightful comments on the manuscript.

GRANTS

This work was supported by a grant from the Canadian Institutes of Health Research (MOP-79352) to C. C. Pack and a fellowship from the National Science and Engineering Research Council (PGS D3-362469-2008) to J. M. G. Tsui.

DISCLOSURES

No conflicts of interest, financial or otherwise, are declared by the author(s).

REFERENCES

Allman J, Miezin F, McGuinness E. Direction- and velocity-specific responses from beyond the classical receptive field in the middle temporal visual area (MT). *Perception* 14: 105–126, 1985.

Anderson JS, Lampl I, Gillespie DC, Ferster D. Membrane potential and conductance changes underlying length tuning of cells in cat primary visual cortex. *J Neurosci* 21: 2104–2112, 2001.

Anderson SJ, Burr DC. Receptive field size of human motion detection units. *Vision Res* 27: 621–635, 1987.

Anderson SJ, Burr DC. Receptive field properties of human motion detector units inferred from spatial frequency masking. *Vision Res* 29: 1343–1358, 1989.

Angelucci A, Levitt JB, Walton EJ, Hupe JM, Bullier J, Lund JS. Circuits for local and global signal integration in primary visual cortex. *J Neurosci* 22: 8633–8646, 2002.

Atick JJ. Could information theory provide an ecological theory of sensory processing? *Network Comp Neural* 3: 213–251, 1992.

Berezovskii VK, Born RT. Specificity of projections from wide-field and local motion-processing regions within the middle temporal visual area of the owl monkey. *J Neurosci* 20:1157–1169, 2000.

Betts LR, Sekuler AB, Bennett PJ. Spatial characteristics of center-surround antagonism in younger and older adults. *J Vis* 9: 25.1.151157–25, 2009.

Born RT. Center-surround interactions in the middle temporal visual area of the owl monkey. *J Neurophysiol* 84: 2658–2669, 2000.

Born RT, Tootell RB. Segregation of global and local motion processing in primate middle temporal visual area. *Nature* 357: 497–499, 1992.

Born RT, Bradley DC. Structure and function of visual area MT. *Annu Rev Neurosci* 28: 157–189, 2005.

Born RT, Groh JM, Zhao R, Lukasewycz SJ. Segregation of object and background motion in visual area MT: effects of microstimulation on eye movements. *Neuron* 26: 725–734, 2000.

Buracas GT, Albright TD. Contribution of area MT to perception of three-dimensional shape: a computational study. *Vision Res* 36: 869–887, 1996.

Cadieu C, Kouh M, Pasupathy A, Connor CE, Riesenhuber M, Poggio T. A model of V4 shape selectivity and invariance. *J Neurophysiol* 98:1733–1750, 2007.

Cavanaugh JR, Bair W, Movshon JA. Nature and interaction of signals from the receptive field center and surround in macaque V1 neurons. *J Neurophysiol* 88: 2530–2546, 2002.

Chen Y, Geisler WS, Seidemann E. Optimal decoding of correlated neural population responses in the primate visual cortex. *Nat Neurosci* 9: 1412–1420, 2006.

Churan J, Richard AG, Pack CC. Interaction of spatial and temporal factors in psychophysical estimates of surround suppression. *J Vis* 9: 15.11.151412–15, 2009.

Churan J, Khawaja FA, Tsui JM, Pack CC. Brief motion stimuli preferentially activate surround-suppressed neurons in macaque visual area MT. *Curr Biol* 18: R1051–R1052, 2008.

DeAngelis GC, Uka T. Coding of horizontal disparity and velocity by MT neurons in the alert macaque. *J Neurophysiol* 89: 1094–1111, 2003.

DeAngelis GC, Freeman RD, Ohzawa I. Length and width tuning of neurons in the cat's primary visual cortex. *J Neurophysiol* 71: 347–374, 1994.

DeAngelis GC, Robson JG, Ohzawa I, Freeman RD. Organization of suppression in receptive fields of neurons in cat visual cortex. *J Neurophysiol* 68: 144–163, 1992.

Gautama T, Van Hulle MM. Function of center-surround antagonism for motion in visual area MT/V5: a modeling study. *Vision Res* 41: 3917–3930, 2001.

Gieselmann MA, Thiele A. Comparison of spatial integration and surround suppression characteristics in spiking activity and the local field potential in macaque V1. *Eur J Neurosci* 28: 447–459, 2008.

Golomb JD, McDavitt JR, Ruf BM, Chen JI, Saricicek A, Maloney KH, Hu J, Chun MM, Bhagwagar Z. Enhanced visual motion perception in major depressive disorder. *J Neurosci* 29: 9072–9077, 2009.

Hartline HK. The receptive fields of optic nerve fibers. *Am J Physiol* 130: 690–699, 1940.

Heeger DJ. Normalization of cell responses in cat striate cortex. *Vis Neurosci* 9: 181–197, 1992.

Henrie JA, Shapley RM. The relatively small decline in orientation acuity as stimulus size decreases. *Vision Res* 41: 1723–1733, 2001.

Henrie JA, Shapley R. LFP power spectra in V1 cortex: the graded effect of stimulus contrast. *J Neurophysiol* 94: 479–490, 2005.

Hubel DH, Wiesel TN. Receptive fields and functional architecture in two nonstriate visual areas (18 and 19) of the cat. *J Neurophysiol* 28: 229–289, 1965.

Hunter JN, Born RT. Stimulus-dependent modulation of suppressive influences in MT. *J Neurosci* 31: 678–686, 2011.

Ichida JM, Schwabe L, Bressloff PC, Angelucci A. Response facilitation from the "suppressive" receptive field surround of macaque V1 neurons. *J Neurophysiol* 98: 2168–2181, 2007.

Kapadia MK, Westheimer G, Gilbert CD. Dynamics of spatial summation in primary visual cortex of alert monkeys. *Proc Natl Acad Sci USA* 96: 12073–12078, 1999.

Kaplan E, Shapley RM. The primate retina contains two types of ganglion cells, with high and low contrast sensitivity. *Proc Natl Acad Sci USA* 83: 2755–2757, 1986.

Khawaja FA, Tsui JM, Pack CC. Pattern motion selectivity of spiking outputs and local field potentials in macaque visual cortex. *J Neurosci* 29: 13702–13709, 2009.

Levitt JB, Lund JS. Contrast dependence of contextual effects in primate visual cortex. *Nature* 387: 73–76, 1997.

Movshon JA, Newsome WT. Visual response properties of striate cortical neurons projecting to area MT in macaque monkeys. *J Neurosci* 16: 7733–7741, 1996.

Murphy BK, Miller KD. Balanced amplification: a new mechanism of selective amplification of neural activity patterns. *Neuron* 61: 635–648, 2009.

Pack CC, Hunter JN, Born RT. Contrast dependence of suppressive influences in cortical area MT of alert macaque. *J Neurophysiol* 93: 1809–1815, 2005.

Polat U, Mizobe K, Pettet MW, Kasamatsu T, Norcia AM. Collinear stimuli regulate visual responses depending on cell's contrast threshold. *Nature* 391: 580–584, 1998.

Priebe NJ, Churchland MM, Lisberger SG. Constraints on the source of short-term motion adaptation in macaque area MT. I. The role of input and intrinsic mechanisms. *J Neurophysiol* 88: 354–369, 2002.

Raiguel S, Van Hulle MM, Xiao DK, Marcar VL, Orban GA. Shape and spatial distribution of receptive fields and antagonistic motion surrounds in the middle temporal area (V5) of the macaque. *Eur J Neurosci* 7: 2064–2082, 1995.

Royden CS. Computing heading in the presence of moving objects: a model that uses motion-opponent operators. *Vision Res* 42: 3043–3058, 2002.

Rust NC, Mante V, Simoncelli EP, Movshon JA. How MT cells analyze the motion of visual patterns. *Nat Neurosci* 9: 1421–1431, 2006.

Sceniak MP, Hawken MJ, Shapley R. Visual spatial characterization of macaque V1 neurons. *J Neurophysiol* 85: 1873–1887, 2001.

Sceniak MP, Ringach DL, Hawken MJ, Shapley R. Contrast's effect on spatial summation by macaque V1 neurons. *Nat Neurosci* 2: 733–739, 1999.

Schwabe L, Obermayer K, Angelucci A, Bressloff PC. The role of feedback in shaping the extra-classical receptive field of cortical neurons: a recurrent network model. *J Neurosci* 26: 9117–9129, 2006.

Sclar G, Maunsell JH, Lennie P. Coding of image contrast in central visual pathways of the macaque monkey. *Vision Res* 30: 1–10, 1990.

Shushruth S, Ichida JM, Levitt JB, Angelucci A. Comparison of spatial summation properties of neurons in macaque V1 and V2. *J Neurophysiol* 102: 2069–2083, 2009.

Tadin D, Lappin JS. Optimal size for perceiving motion decreases with contrast. *Vision Res* 45: 2059–2064, 2005.

Tadin D, Lappin JS, Gilroy LA, Blake R. Perceptual consequences of centre-surround antagonism in visual motion processing. *Nature* 424: 312–315, 2003.

Tadin D, Kim J, Doop ML, Gibson C, Lappin JS, Blake R, Park S. Weakened center-surround interactions in visual motion processing in schizophrenia. *J Neurosci* 26: 11403–11412, 2006.

Tanaka K, Hikosaka K, Saito H, Yukie M, Fukada Y, Iwai E. Analysis of local and wide-field movements in the superior temporal visual areas of the macaque monkey. *J Neurosci* 6: 134–144, 1986.

Tsui JM, Cipriani RM, Pack CC. Contrast dependence of center-surround interactions in macaque visual area MT. Program no. 588.15. In: *Society for Neuroscience,* Chicago, IL, 2009.

Tsui JM, Hunter JN, Born RT, Pack CC. The role of V1 surround suppression in MT motion integration. *J Neurophysiol* 103: 3123–3138, 2010.

Xiao DK, Raiguel S, Marcar V, Orban GA. The spatial distribution of the antagonistic surround of MT/V5 neurons. *Cereb Cortex* 7: 662–677, 1997.

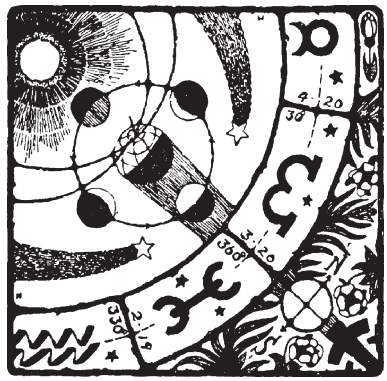

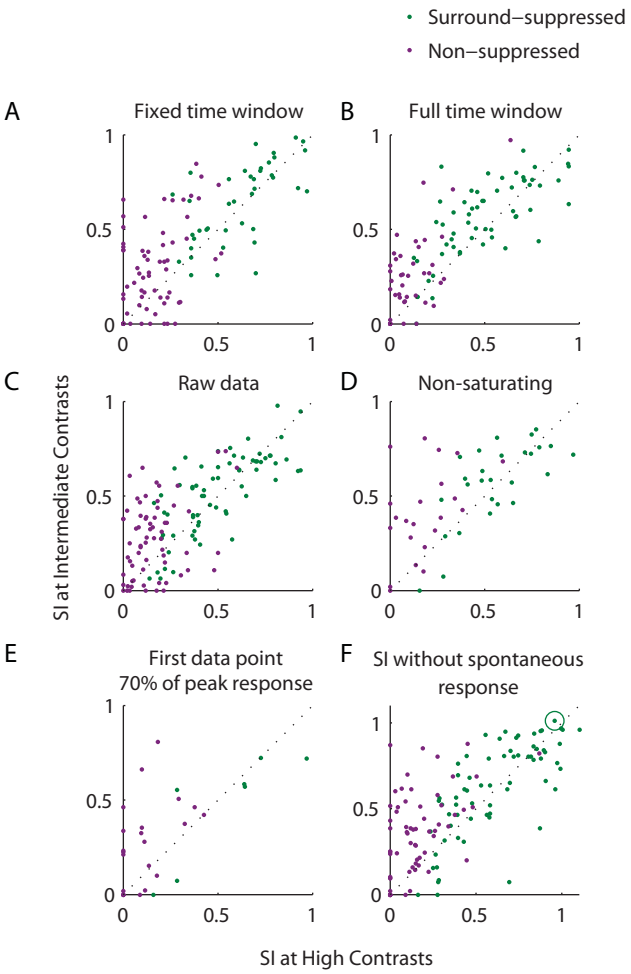

Supplemental Figure 1

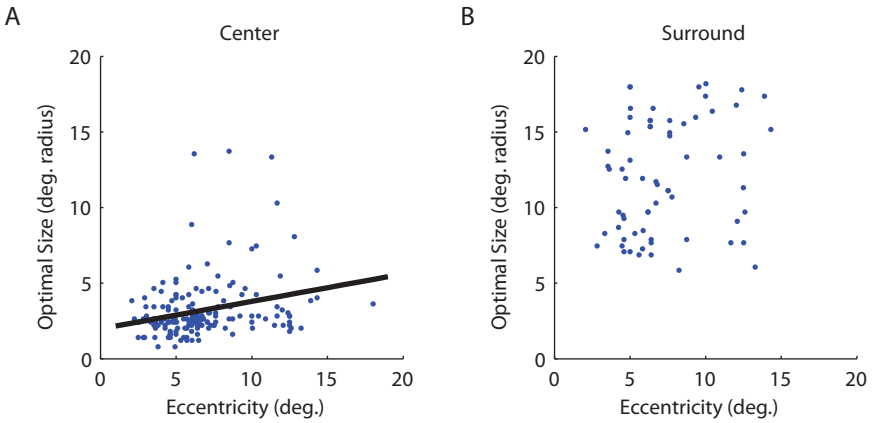

Supplemental Figure 2

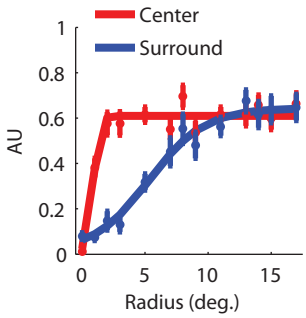

Supplemental Figure 3

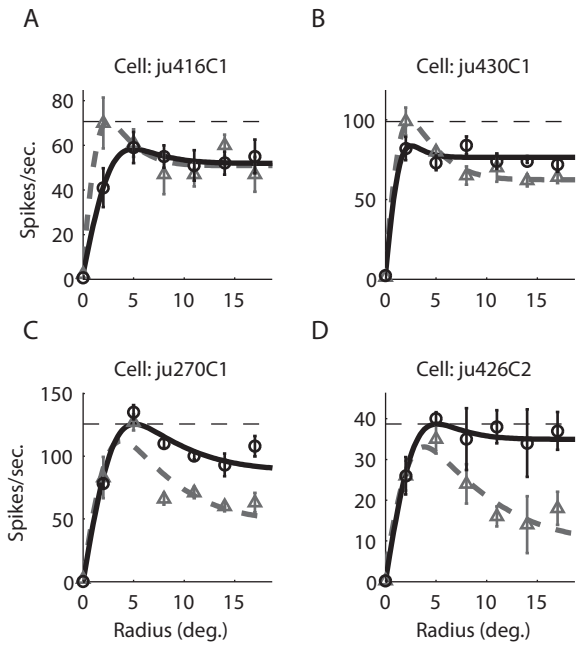

Supplemental Figure 4

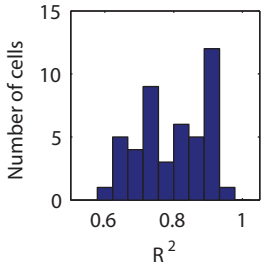

Supplemental Figure 5

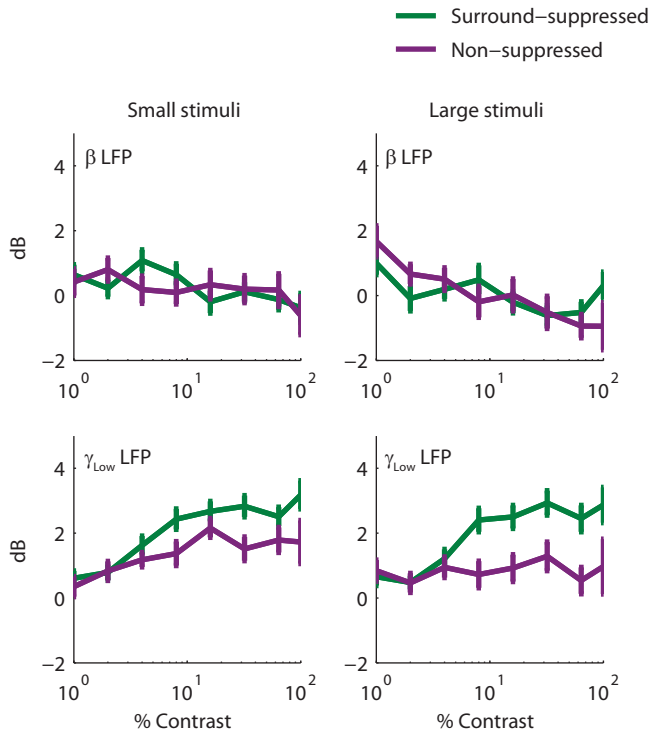

Supplemental Figure 6

Supplemental Figures Captions

Supplemental Figure 1 – Control analyses. **A:** Same as Figure 1b, but the responses were calculated from the last 200 ms before stimulus offset. **B:** Same as Figure 1b, but the responses were calculated from a window sized to the entire duration of the stimulus. **C:** Same as Figure 1b, but the SI was calculated using the raw data points instead of DOG fits. **D:** Same as Figure 1b, but only for those cells whose peak response did not occur at the highest measured contrast. **E:** Same as Figure 1b, but only for those cells whose response at the first sampled size was less than 70% of the peak response. **F:** Same as Figure 1b, but with the spontaneous response removed before computing the SI. The open circle corresponds to the cell shown in Figure 3b.

Supplemental Figure 2 – Relationship between optimal size and eccentricity. Here, the optimal sizes are computed by fitting the size tuning curves at high contrast to the DOG model. The reported sizes correspond to the points at which the excitatory and inhibitory error functions (equation 2 in the paper) reach 95% of their maximum values. This criterion prevents overestimating receptive field size in neurons for which the size-tuning curve plateaus, although it leads to slightly smaller estimated receptive field sizes. **A:** The optimal size for the excitatory center receptive field plotted against eccentricity. The results are correlated (Spearman's rho; $r = 0.2701$, $p = 0.0004$). Solid line shows the regression line. Mean receptive field eccentricity is 6.7 degrees; mean center optimal size is 3.2 degrees radius (n=171). **B:** Same as A, but for the surround. Only the cells that were significantly surround-suppressed are shown. Mean surround optimal size is 12.04 degrees (n=67).

Supplemental Figure 3 – The average size response functions for the centers and surrounds, examined non-parametrically by fitting the size parameter in equation (6) separately for each size. The red and blue solid dots are the mean size responses extracted from the model fits, and the solid lines are the fits of the results to a sigmoidal function (equation 7).

Supplemental Figure 4 – Effect of stimulus contrast on surround suppression for 4 MT cells. **A:** The effect of contrast is driven by a decrease in the response at the optimal size as contrast increases from intermediate (5%; triangle symbols) to high (100%; open circles). The horizontal dashed line shows the peak response of the cell (see also Figure 2b). **B:** In addition to the decrease in response at the optimal size, the neural response also increases at the largest sizes as contrast increases from intermediate (10%; triangle symbols) to high (100%; open circles). **C:** An example cell whose peak response at high contrast (100%; open circles) is not at the first sampled size. Surround suppression still emerges at intermediate contrast (10%; triangle symbols). **D:** Same as C, but for another example cell (100%; open circles, 5%; triangle symbols).

Supplemental Figure 5 – Distributions of Variance Accounted For, R^2 for the subset of data for which at least 7 different contrasts were tested.

Supplemental Figure 6 – Mean contrast response functions for LFPs recorded at suppressed (green) and non-suppressed (purple) sites. The first row shows the beta band

(16-24 Hz) LFP results. There is little difference between the surround-suppressed and the non-suppressed population. The second row shows the LFPs for the γ_{low}. Results are similar to the γ_{high} band, as shown in Figure 9.

Supplemental Table 1

Parameters	Description	Non-suppressed $\mu \pm \delta$	Surround-suppressed $\mu \pm \delta$	t-test p-values
Excitatory parameters				
Contrast response				
k_e	Gain	67.06 ± 27.32	91.79 ± 40.00	p = 0.026*
n	Slope	0.99 ± 0.21	0.89 ± 0.21	p = 0.113
c_{50n}	Semi-saturation constant	2.37 ± 0.75	2.23 ± 0.58	p = 0.478
R_0	Spontaneous firing rate	4.70 ± 4.82	3.56 ± 7.04	p = 0.549
Size response				
k_a	Gain	0.45 ± 0.11	0.48 ± 0.14	p = 0.547
a_n	Slope	2.58 ± 0.93	3.93 ± 1.33	p < 0.001**
a_{50}	Response threshold	1.36 ± 0.49	1.00 ± 0.49	p = 0.020*
a_0	Baseline response	0.00 ± 0.00	0.00 ± 0.00	p = 0.614
Inhibitory parameters				
Contrast response				
k_i	Gain	28.02 ± 11.34	59.92 ± 25.77	p < 0.001**
m	Slope	2.11 ± 0.67	1.28 ± 0.76	p < 0.001**
c_{50m}	Semi-saturation constant	3.32 ± 1.88	2.88 ± 0.72	p = 0.265
Size response				
k_b	Gain	0.35 ± 0.12	0.37 ± 0.09	p = 0.646
b_n	Slope	1.00 ± 0.64	1.23 ± 0.48	p = 0.162
b_{50}	Response threshold	6.48 ± 3.67	6.24 ± 1.67	p = 0.761
b_0	Baseline response	0.08 ± 0.06	0.03 ± 0.04	p = 0.003**

μ: average, δ: standard deviation, * and ** indicate significant p values.